# Vault Nanocapsule Dissociation into Halves Triggered at Low pH†

Lisa E. Goldsmith,‡,§ Marcella Yu,‡,§ Leonard H. Rome,||,⊥ and Harold G. Monbouquette*,‡,⊥

*Chemical and Biomolecular Engineering Department, Department of Biological Chemistry, and California NanoSystems Institute, University of California, Los Angeles, California 90095*

*Received March 29, 2006; Revised Manuscript Received December 16, 2006*

ABSTRACT: Vaults are self-assembled ribonucleoprotein nanocapsules that consist of multiple copies of three proteins (major vault protein, VPARP, and TEP1) and an untranslated RNA. Although their function has not been determined, vaults are found in nearly all eukaryotic cells. This study describes the use of fluorescence spectroscopy, multiangle laser light scattering (MALLS), and the quartz crystal microbalance (QCM) as tools in investigating recombinant vault conformational change in response to a varied solution pH. Identification of conditions for reversible vault disassembly and reassembly could enable application of these nanocapsules in drug delivery and in nanomaterials synthesis. Initial monitoring of changes in the intrinsic fluorescence intensity of vaults showed a 60% increase at pH 3.4 compared to that at pH 6.5, suggesting vaults exhibit a more open conformation at low pH. Fluorescence quenching studies provided further evidence of a vault structural change at low pH. MALLS data suggested a decrease in molecular mass accompanied by a clear increase in the radius of gyration as the solution pH was shifted from 6.5 to 3.4. This result prompted the hypothesis that vaults dissociate at least partially at low pH. Using the QCM to study adsorption of the vault onto self-assembled monolayers, data that suggest vault dissociation at low pH, even when the vault is in an adsorbed state, were also obtained. Finally, transmission electron microscopy (TEM) of negatively stained vaults at pH 6.5 and 3.4 confirmed the fluorescence spectroscopy, MALLS, and QCM findings by providing visual evidence that vaults disassemble into halves as the solution pH is lowered from 6.5 to 3.4.

Vaults are large, hollow ribonucleoprotein particles (13 ± 1 MDa), which are highly conserved among eukaryotic species (*1*, *2*). Vault particles originally were observed in preparations of clathrin-coated vesicles and were named for their resemblance in structure to arched cathedral ceilings (*3*, *4*). The function of vaults in cells is unknown, but they are thought to play a role in nucleocytoplasmic transport on the basis of their association with the nuclear pore complex and nuclear membranes (*5*, *6*). Recent studies also have suggested that vaults may bind to cell signaling pathway components in vivo (*7*−*12*). Aside from their native role, externally applied vaults are taken up readily by HeLa cells (*13*), possibly through endosomal pathways, suggesting that they may be well suited for drug delivery applications.

Vaults are composed of multiple copies of an untranslated RNA (vRNA) and three proteins: major vault protein (MVP),[1] which makes up 75% of the vault mass; vault poly-(ADP-ribose) polymerase (VPARP); and telomerase-associated protein 1 (TEP1) (*14*). According to cryoelectron microscopy reconstruction images, vaults have a barrel-like shape with maximum dimensions of 72.5 nm × 41 nm × 41 nm (*14*) and an internal volume of $5 \times 10^4$ nm$^3$ (*15*). Their capsular structure gives them the potential to be used as compartments in which to encapsulate, transport, and possibly synthesize materials. Each vault is composed of two identical halves, and 96 copies of MVP (48 in each half) form the backbone of the vault structure (*14*). An illustration of an intact vault, as well as schematics of other vault conformations which will be discussed throughout this work, is presented in Figure 1.

When intact vaults are deposited on polylysine-coated mica and imaged by freeze-etch electron microscopy with platinum shadowing, they appear as flowerlike structures with eight rectangular petals (*2*). These "flowers" are usually seen in pairs, suggesting that each whole vault is composed of two flowers, folded so that the ends of their petals meet along the waist of the vault. It seems likely that vaults in cells open and close in response to cellular signals. However, whether vaults spread fully into flowerlike structures in vivo is unknown.

This study was conducted using recombinant CP-MVP vault particles, which consist of 96 copies of a modified MVP and no other proteins or nucleic acids. Recombinant CP-MVP subunits can self-assemble into vault particles, which

† This work was supported by National Science Foundation NIRT Grant MCB-0210690.

* To whom correspondence should be addressed: Chemical and Biomolecular Engineering Department, University of California, 5531 Boelter Hall, 420 Westwood Plaza, Los Angeles, CA 90095. E-mail: hmonbouq@ucla.edu.

‡ Chemical and Biomolecular Engineering Department.

§ These authors contributed equally to this work.

|| Department of Biological Chemistry.

⊥ California NanoSystems Institute.

[1] Abbreviations: MVP, major vault protein; VPARP, vault poly-(ADP-ribose) polymerase; TEP1, telomerase-associated protein 1; MALLS, multiangle laser light scattering; QCM, quartz crystal microbalance; TEM, transmission electron microscopy; MUA, 11-mercaptoundecanoic acid; BCA, bicinchoninic acid; BSA, bovine serum albumin; SAM, self-assembled monolayer; cryoEM, cryoelectron microscopy.

10.1021/bi0606243 CCC: $37.00 © 2007 American Chemical Society
Published on Web 02/16/2007

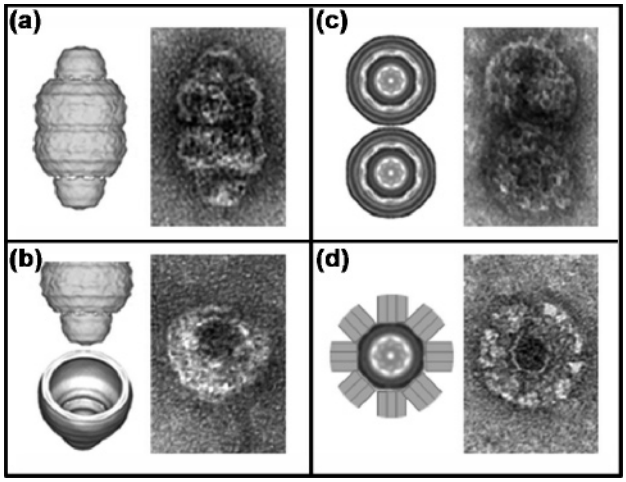


FIGURE 1: Schematic illustrating four vault conformations and their corresponding negative stain electron microscopic images. (a) CryoEM reconstruction of an intact vault particle, side view (left), and negative stain EM of a vault particle, side view (right). (b) Two cryoEM orientations of a half-vault derived from splitting a vault at the waist (left). The bottom half-vault is a slightly skewed image which most closely approximates the negative stain EM half-vault image shown at the right. Negative stain EM of a half-vault (right). (c) CryoEM reconstruction of a half-vault pair, top view (left), and negative stain EM of a half-vault pair (right). (d) A model of a half-vault end-on view which has "opened" into an eight-petal flower, based on the open vaults described in Kedersha et al. (*2*) (left). Negative stain EM image of an open half-vault flower (right) (the flower petals which can be best viewed by freeze-etch platinum shadowing are not visualized as clearly by negative staining).

have been shown to have structures identical to and biochemical characteristics similar to those of endogenous rat vaults (*16*). In these CP-MVP vaults measuring 73.7 nm × 41 nm × 41 nm (*14*), each MVP subunit is appended at its N-terminus with a 12-amino acid peptide derived from the metallothionine protein that contains four cysteine residues. Since all MVP N-termini are found at the vault waist (*14*), it is possible that the cysteine residues of CP-MVP form inter- and/or intrachain disulfide bridges that stabilize the vault structure (*14*). CP-MVP vaults in fact are found to be more stable than wild-type particles, with minimal variations in size, shape, and conformation (*14*); however, there is no direct evidence to implicate a role for disulfide bridges in improved vault stability. Although CP-MVP vault samples purified using sucrose gradients (*14*, *16*) are the most stable of all recombinant and native vault types prepared to date, small amounts of aggregated and denatured particles are still visible in CP-MVP preparations (as discussed in Results and Discussion).

Inspired by previous findings of vault dissociation on polylysine-coated surfaces (*2*), our work is the first to employ several experimental tools in the study of vault conformational change in solution in response to low pH. Preliminary ideas for possible means of effecting conformational change in vaults, including exposure to low pH, were obtained from prior studies of structural change induced in viruses by manipulation of their solution environments (*17*−*20*). This study builds on the prior results of others showing the usefulness of fluorescence spectroscopy (*21*−*23*), fluorescence quenching (*24*−*27*), and multiangle laser light scattering (MALLS) (*28*−*34*) for the monitoring of conformational changes of proteins and virus particles. Here, the quartz crystal microbalance (QCM) (*35*−*38*) also has been implemented in the study of conformational changes of adsorbed vaults, and transmission electron microscopy (TEM) is employed as an additional means of confirming the interpretation of fluorescence, MALLS, and QCM data.

Understanding physiological signals that can trigger vault conformational change in solution will provide insight into native vault behavior, which will aid in the design of vaults as drug delivery vehicles whose contents will be released in response to specific conditions in vivo. Since vaults are known to associate with cell signaling pathway components (*7*−*12*), vault conformation may play a key role in cell signaling mechanisms and transport processes. Despite the fact that the details of vault function are unknown, their highly conserved structure across diverse phyla, from worms to humans, strongly suggests an important role that could one day be exploited for therapeutic applications.

## MATERIALS AND METHODS

CP-MVP recombinant vaults were prepared as described previously (*14*, *16*) and were stored at 4 °C in 20 mM MES at pH 6.5 until they were used. In short, the cDNA sequence of MVP was subcloned into a recombinant baculovirus, where it was overexpressed, and then transfected into an Sf9 insect cell line (*14*). Recombinant vaults were extracted from lysed insect cells and purified using centrifugation and a sucrose gradient. They are found mostly in the 40 and 45% sucrose layers, which coincides with natural vaults purified from tissues (*14*, *16*). To change the pH environment of the vaults, vault stock aliquots were diluted at least 15-fold into the desired buffer and were allowed to equilibrate for 1 h.

*Materials.* MES, Tris, L-tryptophan, and 11-mercaptoundecanoic acid (MUA) were obtained from Sigma Chemical Co. (St. Louis, MO). The pH of MES (20 mM, pH 6.5) and 85 mM Tris buffers, prepared in the pH range of 6.5−9.0, was adjusted using 4 M HCl and 4 M NaOH. Citrate-phosphate buffers in the pH range of 2.6−6.5 (total concentration of 55−85 mM) were prepared using anhydrous citric acid and sodium phosphate dibasic heptahydrate (Fisher Chemicals, Fair Lawn, NJ). Acrylamide was purchased from Invitrogen (Carlsbad, CA).

*Fluorescence Spectroscopy.* Intrinsic aromatic amino acid (principally tryptophan) emission spectra (FL3-22, Instruments S.A., Inc., SPEX Division, Edison, NJ) were gathered at a controlled pH at an excitation wavelength of 295 nm and were background-corrected. In studies of intrinsic fluorescence quenching by acrylamide, aliquots of a 2 M acrylamide stock were added to the pH-buffered vault solution, which was allowed to equilibrate for 10 min before spectra were recorded as described above. Spectra were corrected for the inner filter effect due to acrylamide adsorption at the excitation and appropriate emission wavelengths (*39*).

For proteins, emission is heterogeneous and the appropriate equation for the fraction of tryptophan (Trp) fluorescence quenched (*40*) is

$$\frac{F_0 - F}{F_0} = \sum_i \frac{f_i K_{Qi}[Q]}{1 + K_{Qi}[Q]} \quad (1)$$

where $F_0$ is the peak fluorescence emission intensity of vaults in the absence of quencher, $F$ is the fluorescence intensity

in the presence of acrylamide at a molar concentration ([Q]), $f_i$ is the fractional contribution of component $i$ to the total fluorescence, and $K_{Qi}$ is the collisional quenching constant (inverse molar), also called the Stern−Volmer constant, of component $i$. For proteins containing multiple Trp residues (for example, each CP-MVP vault particle contains 576), eq 1 can be expanded for the $i$ residues. Since fitting the expanded form of eq 1 is not practical for vaults, we make the approximation that at low quencher concentrations, $[Q]^2$ and higher-order terms may be eliminated. Therefore, peak fluorescence intensity data at low acrylamide concentrations (<0.2 M) were fit to a percent quenching model for multiple Trp-containing proteins derived by Lehrer (*40*) using a nonlinear least-squares algorithm (Sigma Plot 2000 version 6.00):

$$\frac{F_0 - F}{F_0} = 100\frac{(f_a)_{eff}(K_Q)_{eff}[Q]}{1 + (K_Q)_{eff}[Q]} \qquad (2)$$

where $(f_a)_{eff}$ is the "effective" maximum fraction of Trp residues accessible to the quencher [limited to $0 \leq (f_a)_{eff} \leq 1$] and $(K_Q)_{eff}$ is the effective collisional quenching constant (inverse molar) for all Trp residues in the protein, which is related to the frequency of the collisions between acrylamide and excited Trp residues (*27*, *40*). In such analyses at low quencher concentrations, the calculated effective parameters will be weighted toward those Trp residues with large $f_iK_{Qi}$ values which are more easily accessible (*40*).

*Multiangle Laser Light Scattering (MALLS).* Static scattered light intensity measurements (DAWN DSP model F, Wyatt Technology, Santa Barbara, CA) were carried out in batch mode. A 5 mW He−Ne laser at 632.8 nm served as the vertically polarized light source, and light scattered by the sample was detected by 18 photodiodes at angular positions ranging from 26.56° to 144.46°. All buffer used for MALLS experiments was prefiltered (0.02 $\mu$m, Whatman Anotop 25 Plus).

In studies of the effect of low pH on vaults, vault preparations were divided equally for parallel experimental analysis at pH 6.5 and 3.4. For a single trial, a CP-MVP sample containing ~0.25−0.35 mg of total vault protein was added to 10 mL of the desired buffer, and the system was allowed to equilibrate for 1 h. After the sample had been mixed, the sample solution was filtered (0.2 $\mu$m, Nalgene syringe filter, SFCA) directly into a clean 20 mL scintillation vial. The vial containing the sample solution then was used directly for MALLS data collection.

Scattered light intensities were recorded with ASTRA (version 4.90.07, Wyatt Technology). Light scattering data at the highest vault concentration were collected over four 1 min intervals, with the vial rotated by a quarter turn between each minute to average over minor vial glass imperfections. Samples then were diluted 20% with additional filtered buffer. After the samples had been mixed for 5 min followed by 0.2 $\mu$m filtration, a new set of scattered light intensity measurements were collected as described above. This procedure was repeated to obtain MALLS data at four different concentrations for each vault sample.

A classic Zimm plot analysis was then conducted. The light scattering theory of Zimm and Debye relates the time-averaged, scattered light intensities with the apparent molecular mass and radius of gyration of the scatterer (*41*−*44*). The working equation used to construct a Zimm plot is given as (*42*, *45*)

$$\frac{K^*c}{R_\theta} = \frac{1}{M_W}\left[1 + \frac{16\pi^2 {R_G}^2}{3\lambda^2}\sin^2\left(\frac{\theta}{2}\right)\right] + 2A_2c \qquad (3)$$

where $R_\theta$ is the Rayleigh ratio (*43*) defined as $(I_S/I_0)[r^2/(1 + \cos^2\theta)]$, $I_S$ is the scattered light intensity, $I_0$ is the incident light intensity, $r$ is the distance between the sample compartment and photodiodes, and $\theta$ is the scattering angle. Additional terms in eq 3 are defined as follows. $c$ is the concentration of the scatterer in the solvent (grams per milliliter). $M_W$ is the apparent molecular mass of the macromolecular assembly. $R_G$ is the radius of gyration. $\lambda$ is the wavelength measured in the scattering medium. $A_2$ is the second virial coefficient. $K^*$, defined as $4\pi^2 n_0^2 (dn/dc)^2/(\lambda_0^4 N_A)$, is a function of optical constants, where $n_0$ is the index of refraction of the solvent at the incident radiation (vacuum) wavelength, $\lambda_0$ is the wavelength of the incident radiation (vacuum) beam, $N_A$ is Avogadro's number, and $dn/dc$ is the differential change in the refractive index of the solution with a change in scatterer concentration. Since the CP-MVP vaults used here consist solely of protein, the literature $dn/dc$ value of 0.184 mL/g, which commonly is used for proteins and virus particles, was applied (*28*, *46*).

Zimm plots were generated by plotting $K^*c/R_\theta$ against $\sin^2(\theta/2) + kc$, where $k$ is an arbitrary scaling constant to adjust the spread of the plot (*43*, *44*). The plots consist of multiple concentration and angle lines extrapolated to zero concentration and zero angle. Estimates of $R_G$, $M_W$, and $A_2$ are obtained from the extrapolated zero concentration and zero angle lines.

*Vault Concentration Measurement.* Vault concentrations were determined using a slightly modified micro BCA protein assay (Pierce, Rockford, IL) in which samples were incubated at 37 °C for 2 h instead of the recommended 60 °C for 1 h to reduce the amount of protein precipitation. Actual vault concentrations were determined from a correlation of the micro BCA assay result to vault, rather than bovine serum albumin, concentration. Vault concentrations for the standard curve were determined from the absorbance at 280 nm according to the Beer−Lambert law (Ocean Optics, Dunedin, FL). The molar absorption coefficient of unfolded vault was calculated on the basis of amino acid composition, which then was corrected for folded vault protein using the absorbances of both folded and unfolded vaults at 280 nm (*47*, *48*).

*Quartz Crystal Microbalance (QCM).* In a quartz crystal microbalance (QCM), an oscillating electric potential propagates an acoustic wave across the nonconducting quartz crystal surface whose properties are affected by changes in adsorbed mass (*49*). Changes in the frequency of the quartz crystal oscillation, $\Delta f$ (hertz), can be correlated to changes in adsorbed mass per unit area (*49*, *50*) according to the Sauerbrey equation (*51*), provided the adlayer is thin and rigid and does not slip at the interface. When operated in a liquid system, the fluid becomes coupled to the crystal oscillation. The added viscosity and density of the fluid decrease the resonant frequency of the crystal oscillation (*52*) and contribute to a damping of the oscillation amplitude in the form of viscous losses, which are represented as an increase in the series resonant resistance, $\Delta R$ (ohms), of the

QCM oscillator (*53*). Following crystal equilibration in the liquid, subsequent frequency and resistance changes due to protein adsorption and further manipulation of the adsorbed protein layer can be monitored simultaneously (*35*). It is important to note that for a viscoelastic protein layer that clearly does not obey the Sauerbrey equation, frequency changes due to protein adsorption cannot be directly converted into values of adsorbed mass. Therefore, whenever we discuss "mass" in conjunction with QCM frequency shifts, we mean the "effective mass load" of the protein adlayer (*37*).

The QCM substrates were prepared as described below. The gold surface coatings on 5 MHz, AT-cut quartz QCM crystals (TAN05GLP, Tangidyne Corp., Skaneateles, NY) were cleaned in an oxygen plasma for 10 min. The cleaned substrates then were immersed immediately in absolute ethanol for at least 20 min (*54*) and stored in ethanol until they were used (within 3 weeks). To prepare the gold working surface for self-assembled monolayer (SAM) adsorption, the surface was treated twice with fresh piranha solution (3:1 $H_2O_2/H_2SO_4$ mixture) (**WARNING**: $H_2O_2$ and $H_2SO_4$ are highly corrosive; when mixed, piranha solution becomes hot and is potentially explosive and should therefore be handled with caution and proper protective gear) at room temperature for 1.5 min (*55*), then washed thoroughly with deionized water, and dried in UHP argon. A carboxyl-terminated SAM was formed by exposure of the gold-coated, quartz crystal to 2 mM 11-mercaptoundecanoic acid (MUA) in ethanol overnight. A qualitative assessment of SAM surface coverage was made by comparing cyclic voltammograms of the working gold-coated crystal with and without the SAM in a solution of 50 mM $K_3Fe(CN)_6$ and 1 M NaCl (*56*).

Before measurements were taken, the QCM flow system was equilibrated with the working buffer for ~2 h until the frequency was stable to within 1 Hz. The temperature was kept constant at ~21 °C by immersing the QCM holder and flow lines in a water bath. After initial equilibration, a solution of vaults was added to the equilibrated flow system and recycled until steady conditions were approached (usually ~2 h). After the samples had been rinsed with additional working buffer, the effects of solution conditions on the adsorbed vault adlayer were studied.

The frequency data due to vault adsorption obtained with the QCM (QCM100, Stanford Research Systems, Inc., Sunnyvale, CA) were fit to a four-variable, time-based adsorption model (*57*) to obtain a value for $\psi_2$ (described below) using a five-parameter, double-exponential decay model in SigmaPlot 2000 (version 6.00) of the form $y = y_0 + a\exp(-bt) + c\exp(-dt)$:

$$\Delta f_{ads} = \psi_2 + \frac{k_1\psi_1 - k_2\psi_2}{k_2 - k_1}e^{-k_1 t} + \frac{k_1(\psi_2 - \psi_1)}{k_2 - k_1}e^{-k_2 t} \quad (4)$$

where $\psi_1 = \Delta f^{a}{}_{max}{}^{SA}$ is the saturation due to simple vault adsorption, $\psi_2$ ($=\Delta f^{a}{}_{max}$) is the total frequency change due to vault adsorption and further rearrangement in obtaining a more well-formed adlayer of adsorbed vaults, and $k_1$ and $k_2$ are the rate constants associated with these adsorption steps (*57*). Fitting experimental data in this manner enables determination of the maximum saturation frequency change that can be achieved by vault adsorption, $\Delta f^{a}{}_{max}$.

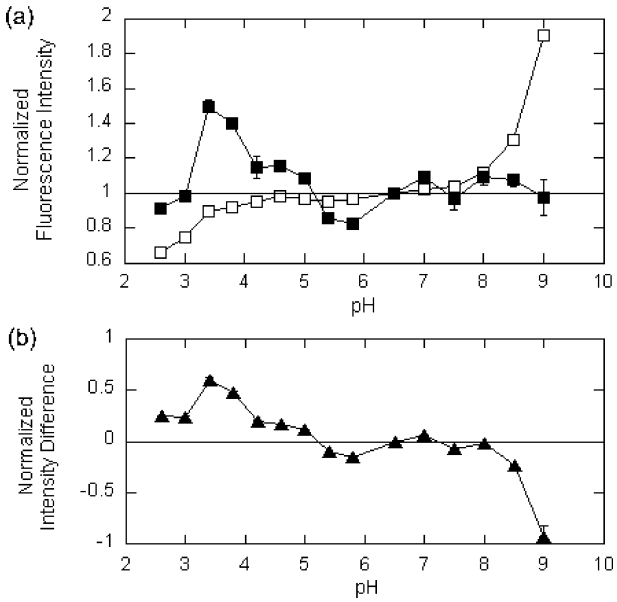


FIGURE 2: (a) Effect of pH on the buffer-subtracted, normalized (to pH 6.5) intrinsic tryptophan fluorescence intensity of 0.1 mg/mL CP-MVP vaults (■) with 0.006 mg/mL free tryptophan (□) as a control. (b) Difference curve (▲) of the normalized fluorescence intensities of CP-MVP vaults subtracted from that of free tryptophan as a function of pH. Excitation was at 295 nm; emission intensities were monitored at a peak wavelength of 345 (CP-MVP) or 365 nm (free Trp).

*Transmission Electron Microscopy (TEM).* To verify vault conformational changes under conditions that have been identified using fluorescence spectroscopy, MALLS, and the QCM, treated vaults were negatively stained and viewed with a JEM1200-EX transmission electron microscope (JEOL, Tokyo, Japan). Vault samples under the desired solution conditions were adsorbed onto nanoporous, carbon-coated copper EM grids at 4 °C by floating the grid upside-down on top of 10−15 $\mu$L drops of sample. After incubation for 5 min, the EM grids with adsorbed vaults were blotted on filter paper and floated on 500 $\mu$L of 1% uranyl acetate for staining, and then blotted and dried on filter paper. TEM images were captured with a BioScan 600W digital camera (Gatan Inc., Pleasanton, CA) using Gatan's DigitalMicrograph (version 3.7.1).

## RESULTS AND DISCUSSION

*Intrinsic Tryptophan Fluorescence.* The effect of solution pH on the peak fluorescence intensity of vaults and free tryptophan, normalized to their intensities at pH 6.5, is shown in Figure 2. Vaults in an open conformation may be expected to exhibit a higher fluorescence intensity and a red-shifted spectrum relative to intact vaults due to increased exposure of aromatic amino acids (principally Trp) that are originally embedded in the vault shell (*39*). Thus, by monitoring the peak intensity and wavelength of vault Trp fluorescence, we can identify conditions under which vaults change conformation.

While the fluorescence intensity of free Trp was roughly constant within the vicinity of neutral pH, it decreased and increased at the low and high pH extremes, respectively, in resemblance to its titration curve ($pK_{a1,COOH} = 2.46$, $pK_{a2,NH_3} = 9.41$), as expected (*58, 59*). Also, as should be expected, the fluorescence intensity versus pH data for vaults were

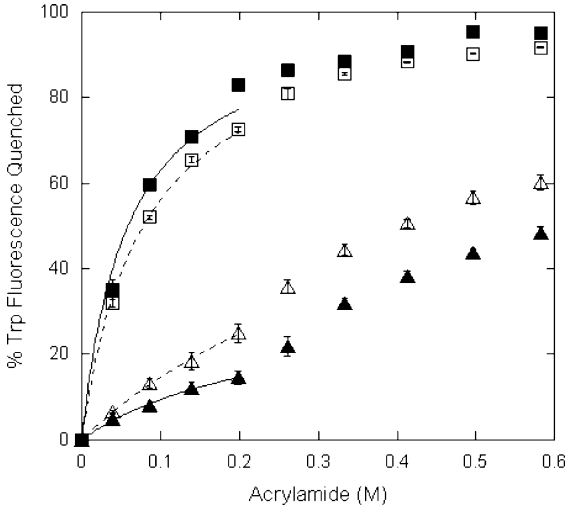


FIGURE 3: Acrylamide quenching of the intrinsic Trp fluorescence in CP-MVP vaults [(▲) pH 6.5 and (△) pH 3.4] with free tryptophan [(■) pH 6.5 and (□) pH 3.4] as a control. Curves at low acrylamide concentrations (<0.2 M) represent the best fit of the data points to the quenching model, eq 2, to obtain values for $(f_a)_{eff}$ and $(K_Q)_{eff}$ as given in the text.

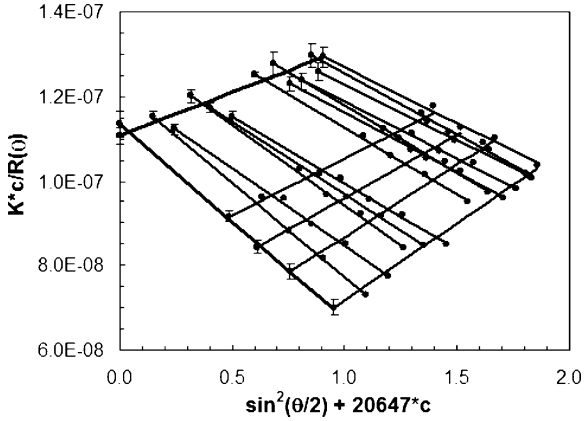


FIGURE 4: Zimm plot based on representative MALLS data for vaults in pH 6.5 buffer. The $R_G$ and $M_W$ values were estimated to be 29 ± 2 nm and 8.9 ± 0.3 MDa, respectively. Excessively noisy data gathered at low angles were not used to construct this Zimm plot.

quite different from those for free Trp; however, the substantial deviation (~60%) in vault fluorescence intensity at pH 3.4 was striking. Although the accompanying red shift in peak emission that was anticipated at pH 3.4 was not large enough to be resolved (data not shown), the change in fluorescence intensity at pH 3.4 suggested a vault conformation change at low pH.

*Fluorescence Quenching.* Acrylamide quenches efficiently (*60*) all excited Trp residues it encounters in a purely random kinetic fashion (*27*), and thus, it is expected that free Trp will be fully accessible to acrylamide, yielding an $(f_a)_{eff}$ of ≈1 in eq 2. Therefore, when vaults are in a more open conformation, acrylamide quenching of vault Trp fluorescence should be enhanced, because the quencher will have improved access to the Trp located within the vault shell, reflected in higher $(f_a)_{eff}$ values. The results of fluorescence quenching studies of vaults versus free tryptophan using acrylamide are shown in Figure 3. Due to heterogeneity of vault emission, only experimental data at <0.2 M Q was fit to eq 2. The heterogeneity arises from Trp residues on the surface and Trp residues buried within the vault, which contribute differently to the total vault protein emission. Therefore, at low Q concentrations, acrylamide quenches the fluorescence of the most easily accessible Trp residues with a high frequency of collision (large value of $f_iK_{Qi}$). However, as more quencher is added, the more shielded residues with lower values of $f_iK_{Qi}$ become increasingly quenched, resulting in the positive deviation from the curve fit at low Q concentrations. Emission of free Trp has also been shown to be heterogeneous (*61*), and we thus also use eq 2 to analyze acrylamide quenching of free Trp.

The data of Figure 3 indicate that the percentage of free Trp fluorescence quenched by acrylamide is slightly lower at pH 3.4 than at pH 6.5. While the effective fractional accessibility $(f_a)_{eff}$ for free Trp was found to be ~1 at both pH values (as expected), the effective quenching constants $[(K_Q)_{eff}]$ were found to be 17 ± 5 and 13 ± 1 $M^{-1}$ at pH 6.5 and 3.4, respectively, by a fit of the data to eq 2. Although acrylamide is able to access and efficiently quench all of the excited free Trp molecules, the lower value of $(K_Q)_{eff}$ for free Trp at low pH may be the result of an increased level of quenching of Trp emission by protons, which would decrease the probability of collisions between acrylamide and excited Trp molecules (*40*).

In contrast, Figure 3 shows that a higher percentage of the Trp present in CP-MVP vaults is quenched at the lower pH than at near-neutral pH. From fits of the data to the quenching model (eq 2), the effective fractional accessibilities $[(f_a)_{eff}]$ for CP-MVP vaults at pH 6.5 and 3.4 were found to be 0.33 ± 0.05 and 0.8 ± 0.1, respectively. The corresponding effective quenching constants $[(K_Q)_{eff}]$ at pH 6.5 and 3.4 were found to be 4 ± 1 and 2.1 ± 0.5, respectively. The approximately ≥2-fold increase in $(f_a)_{eff}$ at low pH suggests that vaults assume a more open conformation at pH 3.4 in which acrylamide has easier access to Trp residues in the vault protein shell, which is in agreement with the intrinsic fluorescence results discussed above. The observed decrease in $(K_Q)_{eff}$ as the pH is lowered from 6.5 to 3.4 may be the result of a decreased frequency of collisions between acrylamide and excited Trp residues in the protein at low pH, as seen for free Trp. Although Trp residues in the vault protein become more accessible to acrylamide at low pH [increase in $(f_a)_{eff}$ as discussed above], protonation of amino acids near the Trp residues may also sterically decrease the frequency of the collisions between acrylamide and Trp residues, further contributing to the decreased value of $(K_Q)_{eff}$ at pH 3.4. Although not shown, quenching of free tryptophan and CP-MVP vaults with $KNO_3$ showed similar trends.

*Multiangle Laser Light Scattering (MALLS).* Further investigation of vault conformational change at low pH was carried out using MALLS due to its utility in estimating the size and shape (i.e., apparent molecular mass and radius of gyration) of macromolecular assemblies. A Zimm plot generated for a representative CP-MVP vault sample at pH 6.5 (Figure 4) yielded estimates for $M_W$ and $R_G$ of 8.9 ± 0.3 MDa and 29 ± 2 nm, respectively. The expected $M_W$ of CP-MVP is approximately 9.3 MDa on the basis of the calculated mass of 96 CP-MVP polypeptides, which agrees roughly with the experimental MALLS result. On the basis of models of the intact vault as a prolate spheroid, a cylinder, and a concentric cylindrical shell, the experimental $R_G$ is expected to fall within the range of 25−30 nm, which it does, thereby

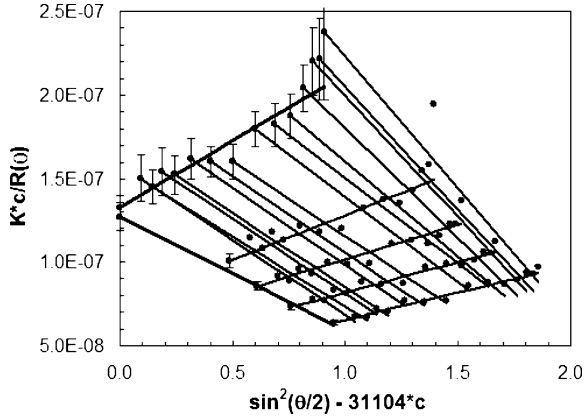


FIGURE 5: Zimm plot based on representative MALLS data for vaults in pH 3.4 buffer. The $R_G$ and $M_W$ values were estimated to be 51 ± 5 nm and 7.7 ± 0.7 MDa, respectively. Excessively noisy data gathered at low angles were not used to construct this Zimm plot.

further confirming the presence of intact vaults in this pH 6.5 sample.

Vault stock solutions used to generate Zimm plots at pH 6.5 were then adjusted to pH 3.4. A representative Zimm plot corresponding to a CP-MVP vault sample in pH 3.4 buffer is shown in Figure 5. In this case, the apparent molecular mass was found to be 7.7 ± 0.7 MDa, and the radius of gyration was 51 ± 5 nm. These values suggest a change in conformation: the marginally discernible decrease in molecular mass offers little support alone to the notion of vault conformational change; however, in combination with the significant increase in the radius of gyration, these results may represent the spreading of the vaults into higher-$R_G$ structures similar to the flowerlike vault halves observed from adsorption onto polylysine-coated mica (*2*). The fact that the apparent molecular mass was not reduced at pH 3.4 may be due to aggregation and the existence of half-vault pairs (Figure 1c), which are two connected half-vaults. Half-vault pairs would retain the same $M_W$ as whole vaults and also account for the increase in $R_G$. These structures will be further discussed in the context of the TEM study.

A total of five different preparations of CP-MVP vaults were divided in two, and MALLS data were gathered at pH 6.5 and 3.4. Figure 6 summarizes the radius of gyration and apparent molecular mass results obtained from the MALLS studies at near-neutral and low pH. As the solution pH was shifted from 6.5 to 3.4, an increase in $R_G$ of ~1.7-fold was observed, indicating a conformational change in the vault structure. However, the average radius of gyration at pH 3.4 was significantly greater than an expected $R_G$ of 44 nm calculated for a spread, flowerlike vault half modeled as a thin disk. The experimental radii of gyration at pH 3.4 could be shifted higher due to vault protein aggregation and half-vault pairs, as the Zimm plot $R_G$ represents the weight-average value for a polydisperse sample. Aggregation and possible half-vault pairs in vault preparations leading to polydispersity also could explain the statistically insignificant change in the apparent molecular mass accompanying the increased radius of gyration at lower pH. Nevertheless, despite significant uncertainty in the apparent $M_W$ values, the MALLS data support qualitatively the hypothesis that whole vaults change conformation at low pH.

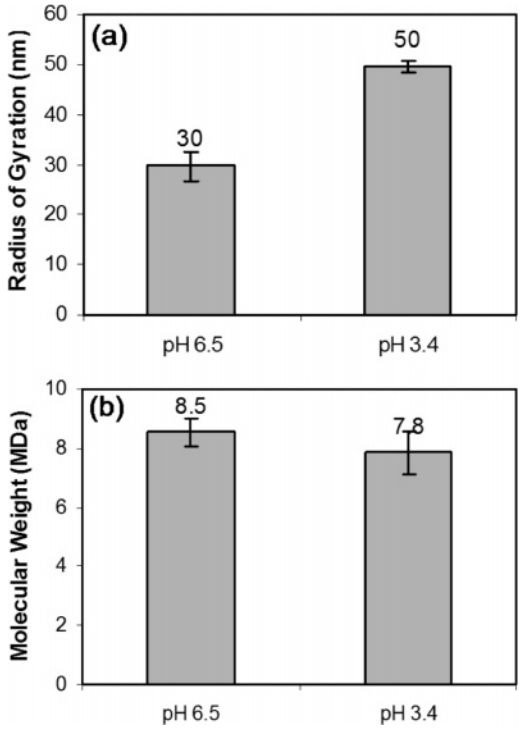


FIGURE 6: (a) Average radii of gyration for five CP-MVP vault preparations at pH 6.5 and 3.4. (b) Average apparent molecular masses for the same five vault preparations at pH 6.5 and 3.4. Error bars represent standard deviations of the means.

*Quartz Crystal Microbalance (QCM).* The QCM was explored as a tool for studying conformational changes of adsorbed vaults in response to pH shifts. By modeling the conformation and water (or buffer) content of the proteins in the adlayer, we can estimate the expected frequency change due to adsorption of a well-formed protein monolayer, $\Delta f_{ML}$, from the adsorbed mass using the Sauerbrey equation (*35*, *37*, *38*). Adsorption of a monolayer of vaults, accounting for the mass of buffer enclosed in the vault interior and 30% associated water on the exterior, should result in an estimated QCM frequency decrease ($\Delta f_{ML}$) between 163 and 289 Hz. This range of values represents the frequency change associated with adsorption of a side-packed and an end-packed monolayer, corresponding to expected vault surface coverages of 2.9 and 5.1 $\mu$g/cm$^2$, respectively. Additionally, the QCM can be used to monitor qualitatively changes in adsorbed vault mass and in vault conformation in response to pH shifts. If low pH results in vault dissociation and removal of one half of each adsorbed vault, the expected frequency increase would be roughly half of the frequency decrease caused by adsorption, depending on how much of the interior water is lost.

Figure 7 shows the typical QCM frequency and resistance response obtained for intact vaults deposited at pH 6.5 onto an 11-carbon, carboxyl-terminated self-assembled monolayer formed from adsorbed MUA. By fitting the initial frequency decrease to the time-based adsorption model given by eq 4, we found the saturation frequency decrease for the adsorption of CP-MVP vaults, $\Delta f^a_{max}$, to be 184 Hz, which falls within the range predicted for a monolayer of CP-MVP vaults ($\Delta f_{ML}$). While it might not be expected that net negatively charged vaults (pI ~5.0) (*3*) would adsorb onto a negatively charged carboxyl-terminated SAM [MUA; p$K_a$ ~ 5.7 (*62*)] at pH 6.5, the observed vault adsorption probably arises as

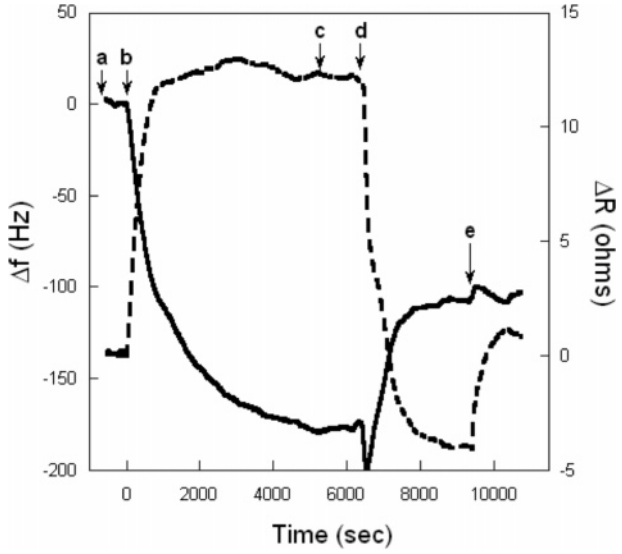


FIGURE 7: Representative QCM data showing intact vault adsorption at pH 6.5 and the subsequent effect of a change in pH on adsorbed vault conformation. Both frequency (—) and resistance (- - -) data are shown as a function of time with pH change of running buffer at the indicated time points [(a, c, and e) pH 6.5, (b) 0.065 mg/mL CP-MVP vaults at pH 6.5, and (d) pH 4.0]. The surface substrate consisted of an 11-carbon, carboxyl-terminated SAM (MUA) on gold.

a result of a combination of local electrostatic interactions, hydrophobic effects, and hydrogen bonding, since vaults do not desorb readily into protein-free running buffer at pH 6.5.

From the QCM data of Figure 7, we surmise that a deposit that approximates a monolayer of whole vaults is adsorbed onto an 11-carbon carboxyl-terminated SAM of MUA at pH 6.5 by noting that the experimental frequency change due to vault adsorption, $\Delta f^{a}_{max}$ of 184 Hz, falls within the range estimated for a monolayer of adsorbed vaults, $\Delta f_{ML}$, between 163 and 289 Hz. The intermediate value of $\Delta f^{a}_{max}$ that was obtained suggests the adsorbed layer may consist of a combination of end- and side-packed particles, or of a non-fully end-packed monolayer due to steric effects between vault particles. At this time, we are unable to determine the exact orientations of adsorbed vault particles, information which may perhaps be obtained in the future by atomic force microscopy measurements in solution. Additionally, the $\Delta f^{a}_{max}$ value on the lower side of the predicted range may perhaps be the result of "the missing mass effect" (*63*), which predicts that the true mass of the protein adlayer is greater than that measured experimentally because viscous losses also contribute to deviations in the adlayer mass predicted by the Sauerbrey equation.

Regardless of the actual orientation of vault particles in the adsorbed layer, upon subsequent exposure to pH 4.0 buffer (Figure 7, point d), which is below the isoelectric point of the vaults, 42% of the initial frequency drop due to adsorption was recovered. Simultaneously, the resistance decrease due to low-pH exposure was large. When the pH was again brought to 6.5 (Figure 7, point e), the frequency change was negligible and was accompanied by an increase in resistance.

The dip in frequency (Figure 7, point d) observed upon exposure of the vault adlayer to pH 4.0 may be attributed to the redistribution of the buffer charges and/or an increase in the mass of the buffer that is coupled to the adsorbed protein layer. For comparison, decreasing the pH of the buffer from 6.5 to 4.0 on the bare MUA SAM (without adsorbed protein) causes a reversible frequency increase of ~12 Hz and a resistance decrease of ~1 Ω (data not shown). After this dip, the frequency increase observed may be caused by the following scenarios.

(1) We hypothesize that the subsequent frequency increase of roughly 50% of the initial decrease due to vault adorption ($\Delta f^{a}_{max}$) indicates dissociation of the vault into halves, with the unbound half being washed away with the running buffer. The large corresponding resistance decrease may be due to a combination of (i) changes in the buffer charges that are coupled to the bound protein adlayer and (ii) a decrease in viscous losses due to a more tightly bound or more rigid half-vault layer. Finally, increasing the pH again to 6.5 (Figure 7, point e) does not cause further desorption of the remaining vault halves (negligible frequency change) but does cause an increase in the observed resistance, again due to points (i) and (ii) above.

(2) Another possible explanation is that upon exposure to low pH, each intact vault disassembles into a pair of half-vaults via a hinge on its waist (Figure 1c). In doing so, an opening vault may force an intact unopened vault off of the surface.

(3) Alternatively, exposure to low pH may not lead to vault dissociation but rather may compress the vaults on the surface, pushing internalized buffer out of the vaults so that it is no longer associated with the protein adlayer, causing the increase in frequency that is observed. Simultaneously, the loss of associated water may cause the protein adlayer to become more rigid (less viscoelastic), producing the observed decrease in the resonant resistance.

On the basis of the QCM results alone, adsorbed vault dissociation due to exposure to low pH cannot be verified since multiple scenarios (1−3 above) may produce qualitatively similar frequency and resistance signal responses. However, TEM results (described below) indicate that vaults, in fact, dissociate into halves when exposed to low pH [both in solution (Figure 9) and in an adsorbed state (Figure 10)], lending credibility to hypothesized scenarios 1 and 2 in describing the QCM results of Figure 7. Similar results showing vault adsorption at pH 6.5 and half-vault desorption at pH 4.0 (and pH 3.4) have been reported for a number of different surfaces, including bare gold, and hydrophobic, amine-terminated, and carboxyl-terminated SAMs of various hydrocarbon chain lengths (data not shown).

*TEM Images.* The techniques discussed above (intrinsic fluorescence, fluorescence quenching, MALLS, and QCM) all suggest that exposure to low pH triggers significant vault conformational change. One possible interpretation of these results, namely, that vaults dissociate into halves at low pH, is visually verified by TEM. Since the most dramatic change was observed by shifting the pH from 6.5 to 3.4, TEM images of vaults that were exposed to low pH in solution and while on the TEM grid were obtained.

Figure 8a shows an image of a typical CP-MVP vault sample deposited from a solution of 20 mM MES buffer (pH 6.5). Most of the vaults exhibited the characteristic barrel-like structure, as depicted in Figure 1a, and appeared to be closed, intact vaults (circled). From random selection of 10 intact vault particles from 10 different fields, a dimension of 70 ± 1 nm × 42 ± 1 nm is estimated according

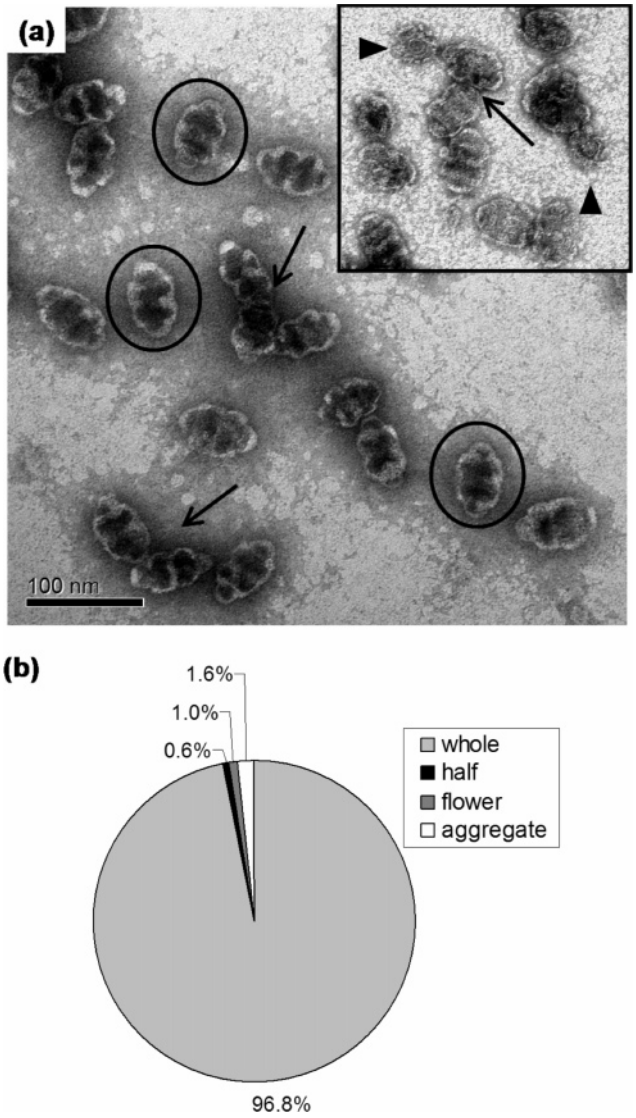


FIGURE 8: (a) TEM image of CP-MVP vaults deposited from 20 mM MES (pH 6.5) buffer. The circles denote intact vaults. Some half-vaults were observed in the sample as shown by the arrowheads. Arrows indicate regions of aggregation. The inset is a TEM image of another area on the grid. (b) Statistics from a total of 690 identifiable vault particles in 31 fields at pH 6.5: whole, whole intact vault; half, upright half-vault; flower, flowerlike half-vault; and aggregate, vault aggregates.

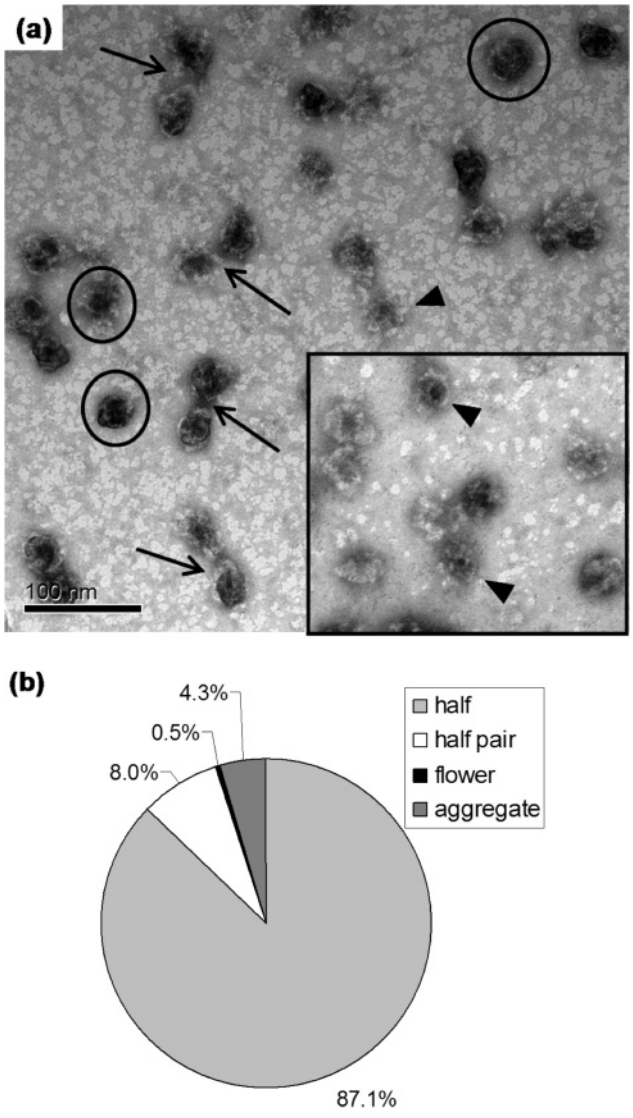


FIGURE 9: (a) TEM images of CP-MVP vaults deposited from citrate-phosphate buffer (pH 3.4) after 60 min. Circles denote single half-vaults. A small amount of half-vaults exhibit spread, flowerlike structures as shown by arrowheads. Arrows indicate half-vault pairs. The boxed insets are images of different locations on the TEM grid. (b) Statistics from a total of 1127 identifiable vault particles in 50 fields at pH 3.4: half, upright half-vault; pair, half-vault pairs; flower, flowerlike half-vault; and aggregate, vault aggregates.

to the scale bar indicated in the figure, which is comparable to the cryoelectron microscopy estimation (*14*). However, some aggregation of whole vaults was observed, as indicated by arrows. A small amount of half-vaults (arrowheads) were found (depicted in Figure 1b,d), indicating that vault samples are not completely homogeneous. The presence of aggregated and dissociated vaults introduces uncertainty into the MALLS analysis at pH 6.5. However, the half-vaults seen in the TEM images might have come from vaults dissociating into halves on the carbon, which may still stay intact in solution.

Statistics for the different structures of vaults observed in TEM images were also compiled for various conditions. The different structures being identified include whole intact vaults (Figure 1a), half-vaults in an upright configuration (Figure 1b), half-vaults in spread, flowerlike configurations (Figure 1d), half-vault pairs (Figure 1c), and obvious vault aggregates. For all conditions, approximately 20% of the entire population cannot be clearly identified as one of the structures listed above. Figure 8b shows the statistics of a total of 690 identifiable vault particles treated under the pH 6.5 condition. More than 96% of those particles appeared as intact vaults, while the remaining particles resembled other structures, including upright half-vaults, flowerlike half-vaults, and vault aggregates. These statistics support the notion of the inherent heterogeneity of vault samples even at pH 6.5, which gives rise to the uncertainties in the MALLS analysis.

Multiple incubation times (5, 10, 20, and 60 min) at pH 3.4 were studied to investigate the effect of low-pH exposure time on vault dissociation. For all incubation times, most of the particles were of half-vault dimensions with an average of $38 \pm 2$ nm $\times$ $34 \pm 1$ nm, thus confirming the vault conformational change at low pH suggested by fluorescence spectroscopy, MALLS, and QCM data. Figure 9a is an image of vaults treated at pH 3.4 in citrate-phosphate buffer for 60 min, which serves as a representative TEM image for all

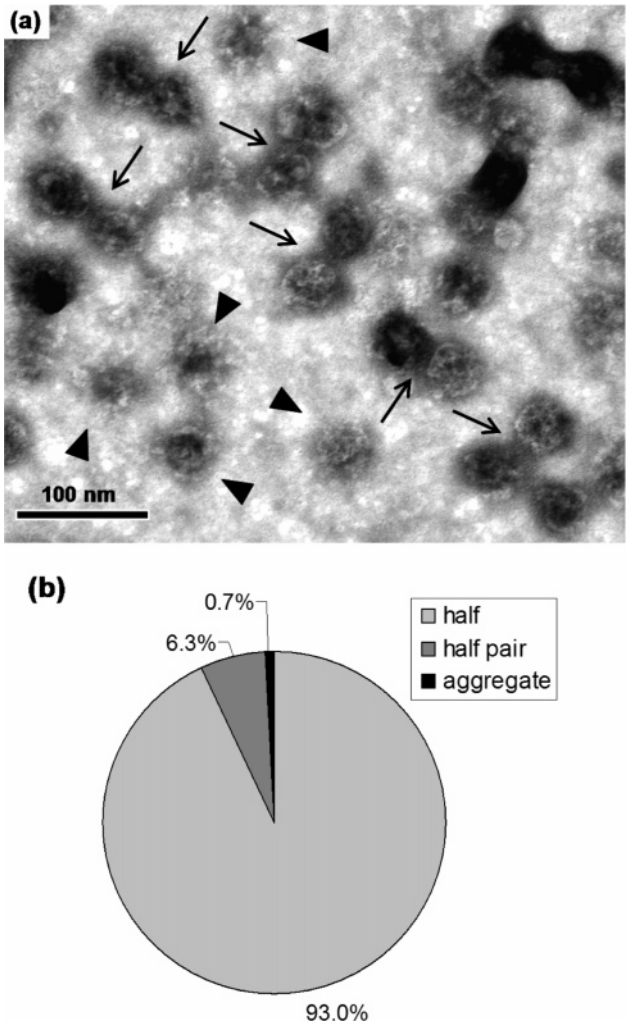


FIGURE 10: CP-MVP vaults adsorbed from pH 6.5 buffer and then exposed to pH 3.4 buffer for 30 s while on grid. (a) TEM image. Arrowheads indicate single half-vaults. Arrows indicate pairs of half-vaults. (b) Statistics from a total of 285 identifiable vault particles in 11 fields: half, upright half-vault; pair, half-vault pairs; and aggregate, vault aggregates.

different incubation times. The observation of half-vaults and the complete lack of whole, intact vaults, even in the 5 min incubation time sample, suggest that vaults disassemble into half-vaults very rapidly upon exposure to pH 3.4 buffer (data not shown). In addition, many half-vaults seemed to exist as pairs (arrows), illustrated in Figure 1c, suggesting that these vaults might stay connected after dissociation triggered by the low pH. A small amount of half-vaults appeared as spread, flowerlike structures, as shown in Figure 1d. Such TEM images are similar to those of the spread, flowerlike vaults on polylysine-coated mica imaged by freeze-etch and platinum shadowing (*2*), although they are not as detailed due to the limitations of the negative-stain procedure. The TEM images under the pH 3.4 condition are less defined compared to the images at pH 6.5, mainly due to the absence of vault inner compartments after dissociation. The inner compartments of vaults at pH 6.5 trapped the uranyl acetate stain, creating a more well-defined and visible intact vault shape.

The statistics of a total of 1127 identifiable vault particles treated under the pH 3.4 condition are illustrated in Figure 9b. The majority of these particles appeared as upright half-vault structures, supporting our analysis of vault dissociation at low pH. Some vaults also seemed to stay connected as half-vault pairs; this structure may represent the dissociation of one intact vault. The amount of aggregation observed under the pH 3.4 condition was also higher than at pH 6.5. Both half-vault pairs and vault aggregates would affect the quality of MALLS data collected at the low pH, as described above in the MALLS results.

To mimic the treatment of vaults on surfaces during QCM experiments, CP-MVP vaults at pH 6.5 were adsorbed onto a carbon TEM grid prior to exposure to pH 3.4 buffer for 30 s by floating the grid upside-down in a pool of the low-pH buffer. The resulting image, shown in Figure 10a, is strikingly similar to the images in Figure 9a, which show vaults that have been deposited onto the grid directly from pH 3.4 buffer. The average dimensions of these half-vault particles measure $40 \pm 1$ nm $\times$ $37 \pm 1$ nm, which again agrees with the expected size of upright half-vaults. The presence of half-vault pairs in samples prepared by both methods may provide some insight into the possible mechanism of vault opening. It appears that when exposed to low pH both in solution and on a grid, vaults unfold at their waists into paired half-vaults, suggesting that these structures may be an intermediate in the process of vault disassembly. TEM images of vaults deposited from solution at pH 3.4 and then exposed to pH 6.5 while on grid (not shown) appeared identical to both vaults adsorbed from solution at pH 3.4 (Figure 9a) and vaults dissociated by exposure to low pH while on grid (Figure 10a). Furthermore, these TEM images lend credibility to hypothesized scenarios 1 and 2 of the QCM results given above, which suggest that adsorbed vaults at pH 6.5 disassemble into halves at low pH, and simultaneously refute scenario 3, in which vaults stay intact but exclude interior buffer.

Figure 10b shows the statistics of a total of 285 identifiable vault particles adsorbed on the TEM grid at pH 6.5 and then subsequently exposed to pH 3.4 while on grid. The relative amounts of different structures estimated for the samples treated at the low pH while on grid are similar to the amounts of samples treated in solution (Figure 9b), confirming vault dissociation triggered by low pH whether the vaults are in solution or in an adsorbed state.

Although TEM offers convincing confirmatory evidence, it is important to recognize that TEM sample preparation entails deposition of samples onto EM grids and subsequent drying before staining and imaging; therefore, the TEM images may not truly reflect the actual conformation or structure of the sample in solution. Furthermore, TEM alone does not allow for efficient screening of a large solution condition parameter space in which to study the effect of solution conditions on vault conformation. Thus, in this work, TEM was used primarily to confirm analyses of fluorescence spectroscopy, MALLS, and QCM data.

The battery of experimental tools that were used provides convincing evidence that vaults dissociate into halves in response to low pH. Although most of the data presented correspond to pH 3.4 and 6.5 due to experimental limitations arising from recombinant vault aggregation near pH 4−5 (data not shown), it is possible that changes in vault conformation begin to occur at pH >4.0. It has been widely documented that the acidic pH of endosomal compartments (pH ~5.0) activates several viral fusion proteins, allowing

fusion of the viral capsids with endocytic membranes and subsequent delivery of viral DNA to the cytoplasm by endosomal lysis (*64*−*66*). Endosomes also may deliver their contents to lysosomes, which are maintained at an even lower pH, normally 4.7−4.8, or a pH as low as 4.5 (*67*). It is possible that vault dissociation in vivo occurs gradually with a decreasing pH, which is consistent with the pH transition associated with cellular entry through the endosomal pathway. Nevertheless, to utilize vaults in drug delivery applications, it is important to identify a physiological condition that can trigger vault dissociation and material release. Since vaults taken up by HeLa cells appeared to enter the lysosomal compartment on the basis of localized fluorescence staining (*13*), the acidic nature of lysosomes may serve as an excellent microenvironment with which to trigger vault dissociation.

Future studies will focus on the encapsulation and release of drugs, including hydrophobic therapeutics. This work will entail an investigation of conditions for reassembly of half-vaults into intact whole vault as well as further study of vault disassembly. Our ultimate goal is to design protocols for reversible vault conformational change to control the encapsulation and release of materials in support of potential applications in drug delivery and in nanomaterials synthesis.

## CONCLUSION

The experimental tools utilized in this paper, fluorescence spectroscopy, MALLS, and the QCM, have proven to be useful collectively in identifying a low-pH condition that triggers vault conformational change. Closed intact vaults observed at pH 6.5 dissociated quickly into half-vaults as the solution pH was decreased to less than 4.0. This vault dissociation phenomenon was confirmed visually by TEM. The dissociation triggered at low pH may become useful for delivery within cellular systems given that endosomes and lysosomes are normally maintained at acidic pH (*64*−*68*). However, specific mechanisms and targets of delivery are beyond the scope of this work.

## ACKNOWLEDGMENT

We thank Dr. Valerie Kickhoefer for sharing her knowledge of vaults, Hedi Roseboro for preparing recombinant vault samples, Dr. Phoebe Stewart for the cryoEM image in Figure 1, and Dr. Bruce Dunn for the use of his oxygen plasma system.

## REFERENCES

1. Kedersha, N. L., Miquel, M.-C., Bittner, D., and Rome, L. H. (1990) Vaults. II. Ribonucleoprotein structures are highly conserved among higher and lower eukaryotes, *J. Cell Biol. 110*, 895−901.
2. Kedersha, N. L., Heuser, J. E., Chugani, D. C., and Rome, L. H. (1991) Vaults. III. Vault ribonucleoprotein particles open into flower-like structures with octagonal symmetry, *J. Cell Biol. 112*, 225−235.
3. Kedersha, N. L., and Rome, L. H. (1986) Isolation and characterization of a novel ribonucleoprotein particle: Large structures contain a single species of small RNA, *J. Cell Biol. 103*, 699−709.
4. Kedersha, N. L., and Rome, L. H. (1986) Preparative agarose gel electrophoresis for the purification of small organelles and particles, *Anal. Biochem. 156*, 161−170.
5. Eichenmuller, B., Kedersha, N., Solovyeva, E., Everley, P., Lang, J., Himes, R. H., and Suprenant, K. A. (2003) Vaults bind directly to microtubules via their caps and not their barrels, *Cell Motil. Cytoskeleton 56*, 225−236.
6. Chugani, D. C., Rome, L. H., and Kedersha, N. L. (1993) Evidence that vault ribonucleoprotein particles localize to the nuclear pore complex, *J. Cell Sci. 106*, 23−29.
7. Yi, C., Li, S., Chen, X., Wiemer, E. A., Wang, J., Wei, N., and Deng, X. W. (2005) Major vault protein, in concert with constitutively photomorphogenic 1, negatively regulates c-Jun-mediated activator protein 1 transcription in mammalian cells, *Cancer Res. 65*, 5835−5840.
8. Kolli, S., Zito, C. I., Mossink, M. H., Wiemer, E. A. C., and Bennett, A. M. (2004) The major vault protein is a novel substrate for the tyrosine phosphatase SHP-2 and scaffold protein in epidermal growth factor signaling, *J. Biol. Chem. 279*, 29374−29385.
9. Mossink, M. H., van Zon, A., Franzel-Luiten, E., Schoester, M., Kickhoefer, V. A., Scheffer, G. L., Scheper, R. J., Sonneveld, P., and Wiemer, E. A. (2002) Disruption of major vault protein (MVP/LRP) gene does not induce hypersensitivity to cytostatics, *Cancer Res. 62*, 7298−7304.
10. Yi, C., Li, S., Wang, J., Wei, N., and Deng, X. W. (2006) Affinity purification reveals the association of WD40 protein constitutive photomorphogenic 1 with the hetero-oligomeric TCP-1 chaperonin complex in mammalian cells, *Int. J. Biochem. Cell Biol. 38*, 1076−1083.
11. Steiner, E., Holzmann, K., Pirker, C., Elbling, L., Micksche, M., Sutterluty, H., and Berger, W. (2006) The major vault protein is responsive to and interferes with interferon-mediated STAT1 signals, *J. Cell Sci. 119*, 459−469.
12. Kim, E., Lee, S., Mian, M. F., Yun, S. U., Song, M., Yi, K. S., Ryu, S. H., and Suh, P. G. (2006) Crosstalk between Src and major vault protein in epidermal growth factor-dependent cell signalling, *FEBS Lett. 273*, 793−804.
13. Kickhoefer, V. A., Garcia, Y., Mikyas, Y., Johansson, E., Zhou, J. C., Raval-Fernandes, S., Minoofar, P., Zink, J. I., Dunn, B., Stewart, P. L., and Rome, L. H. (2005) Engineering of vault nanocapsules with enzymatic and fluorescent properties, *Proc. Natl. Acad. Sci. U.S.A. 102*, 4348−4352.
14. Mikyas, Y., Makabi, M., Raval-Fernandes, S., Harrington, L., Kickhoefer, V. A., Rome, L. H., and Stewart, P. L. (2004) Cryoelectron microscopy imaging of recombinant and tissue derived vaults: Localization of the MVP N termini and VPARP, *J. Mol. Biol. 344*, 91−105.
15. Kong, L. B., Siva, A. C., Rome, L. H., and Stewart, P. L. (1999) Structure of the vault, a ubiquitous cellular component, *Structure 7*, 371−379.
16. Stephen, A. G., Raval-Fernandes, S., Huynh, T., Torres, M., Kickhoefer, V. A., and Rome, L. H. (2001) Assembly of vault-like particles in insect cells expressing only the major vault protein, *J. Biol. Chem. 276*, 23217−23220.
17. Berthet-Colominas, C., Cuillel, M., Koch, M. H. J., Vachette, P., and Jacrot, B. (1987) Kinetic study of the self-assembly of brome mosaic virus capsid, *Eur. Biophys. J. 15*, 159−168.
18. Cuillel, M., Berthet-Colominas, C., Timmins, P. A., and Zulauf, M. (1987) Reassembly of brome mosaic cirus from dissociated virus, *Eur. Biophys. J. 15*, 169−176.
19. Spampinato, C. P., Casati, P., and Andreo, C. S. (1998) Factors affecting the oligomeric state of NADP-malic enzyme from maize and wheat tissues: A chemical crosslinking study, *Biochim. Biophys. Acta 1383*, 245−252.
20. Markovic-Housley, Z., and Garavito, R. M. (1986) Effect of temperature and low pH on structure and stability of matrix porin in micellar detergent solutions, *Biochim. Biophys. Acta 869*, 158−170.
21. Singh, S., and Zlotnick, A. (2003) Observed hysteresis of virus capsid disassembly is implicit in kinetic models of assembly, *J. Biol. Chem. 278*, 18249−18255.
22. Taniguchi, M., and Taniguchi, T. (1975) Thermally induced conformational changes of tobacco mosaic virus and their protein assemblies, *Biochim. Biophys. Acta 386*, 1−17.
23. Permyakov, E. A., and Burstein, E. A. (1984) Some aspects of studies of thermal transitions in proteins by means of their intrinsic fluorescnece, *Biophys. Chem. 19*, 265−271.
24. Pawar, S. A., and Deshpande, V. V. (2000) Characterization of acid-induced unfolding intermediates of glucose/xylose isomerase, *Eur. J. Biochem. 267*, 6331−6338.
25. De Wolf, M. J. S., Van Dessel, G. A. F., Lagrou, A. R., Hilderson, H. J. J., and Dierick, W. S. H. (1987) pH-induced transitions in cholera toxin conformation: A fluorescence study, *Biochemistry 26*, 3799−3806.

26. Busti, P., Scarpeci, S., Gatti, C., and Delorenzi, N. (2002) Use of fluorescence methods to monitor unfolding transitions in $\beta$-lactoglobulin, *Food Res. Int. 35*, 871−877.
27. Eftink, M. R., and Ghiron, C. A. (1976) Exposure of tryptophanyl residues in proteins. Quantitative determination by fluorescence quenching studies, *Biochemistry 15*, 672−680.
28. Santos, N. C., and Castanho, M. A. R. B. (1996) Teaching light scattering spectroscopy: The dimension and shape of tobacco mosaic virus, *Biophys. J. 71*, 1641−1650.
29. Ehrlich, L. S., Liu, T., Scarlata, S., Chu, B., and Carter, C. A. (2001) HIV-1 capsid protein forms spherical (immature-like) and tubular (mature-like) particles in vitro: Structure switching by pH-induced conformational changes, *Biophys. J. 81*, 586−594.
30. Lyles, D. S., McKenzie, M. O., and Hantgan, R. R. (1996) Stopped-flow, classical, and dynamic light scattering analysis of matrix protein binding to nucleocapsids of vesicular stomatits virus, *Biochemistry 35*, 6508−6518.
31. Zlotnick, A., Aldrich, R., Johnson, J. M., Ceres, P., and Young, M. J. (2000) Mechanism of capsid assembly for an icosahedral plant virus, *Virology 277*, 450−456.
32. Tsai, A. M., van Zanten, J. H., and Betenbaugh, M. J. (1998) I. Study of protein aggregation due to heat denaturation: A structural approach using circular dichroism spectroscopy, nuclear magnestic resonanace, and static light scattering, *Biotechnol. Bioeng. 59*, 273−280.
33. Lai, E., and van Zanten, J. H. (2001) Monitoring DNA/poly-L-lysine polyplex formation with time-resolved multiangle laser light scattering, *Biophys. J. 80*, 864−873.
34. Santos, J. L. R., Bispo, J. A. C., Landini, G. F., and Bonafe, C. F. S. (2004) Proton dependence of tobacco mosaic virus dissociation by pressure, *Biophys. Chem. 111*, 53−61.
35. Hook, F., Rodahl, M., Kasemo, B., and Brzezinski, P. (1998) Structural changes in hemoglobin during adsorption to solid surfaces: Effects of pH, ionic strength, and ligand binding, *Proc. Natl. Acad. Sci. U.S.A. 95*, 12271−12276.
36. Nimeri, G., Fredriksson, C., Elwing, H., Liu, L., Rodahl, M., and Kasemo, B. (1998) Neutrophil interaction with protein-coated surfaces studied by an extended quartz crystal microbalance technique, *Colloids Surf., B 11*, 255−264.
37. Hook, F., Rodahl, M., Brzezinski, P., and Kasemo, B. (1998) Energy dissipation kinetics for protein and antibody-antigen adsorption under shear oscillation on a quartz crystal microbalance, *Langmuir 14*, 729−734.
38. Keller, C. A., and Kasemo, B. (1998) Surface specific kinetics of lipid vesicle adsorption measured with a quartz crystal microbalance, *Biophys. J. 75*, 1397−1402.
39. Lacowicz, J. R. (1999) *Principles of Fluorescence Spectroscopy*, 2nd ed., Kluwer Academic/Plenum Publishers, New York.
40. Lehrer, S. S. (1971) Solute perturbation of protein fluorescence. The quenching of tryptophyl fluorescence of model compounds and of lysozyme by iodide ion, *Biochemistry 10*, 3254−3263.
41. Doty, P. M., Zimm, B. H., and Mark, H. (1945) An investigation of the determination of molecular weights of high polymers by light scattering, *J. Chem. Phys. 13*, 159−166.
42. Zimm, B. H. (1948) The scattering of light and the radial distribution function of high polymer solutions, *J. Chem. Phys. 16*, 1093−1099.
43. Tanford, C. (1961) Light Scattering, in *Physical Chemistry of Macromolecules*, pp 275−316, John Wiley & Sons, New York.
44. Zimm, B. H. (1948) Apparatus and methods for measurement and interpretation of the angular variation of light scattering: Preliminary results on polystyrene solutions, *J. Chem. Phys. 16*, 1099−1116.
45. Harding, S. E., and Jumel, K. (1998) Light Scattering, in *Current Protocols in Protein Science* (Coligan, J. E., Dunn, B. M., Ploegh, H. L., Speicher, D. W., and Wingfield, P. T., Eds.) pp 7.8.1−7.8.14, John Wiley & Sons, New York.
46. Vollmer, F., Braun, D., Libchaber, A., Khoshsima, M., Teraoka, I., and Arnold, S. (2002) Protein detection by optical shift of a resonant microcavity, *Appl. Phys. Lett. 80*, 4057−4059.
47. Grimsley, G. R., and Pace, C. N. (2003) Spectrophotometric Determination of Protein Concentration, in *Current Protocols in Protein Science* (Coligan, J. E., Dunn, B. M., Ploegh, H. L., Speicher, D. W., and Wingfield, P. T., Eds.) pp 3.1.1−3.1.9, John Wiley & Sons, New York.
48. Pace, C. N., and Schmid, F. X. (1997) How to Determine the Molar Absorbance Coefficient of a Protein, in *Protein Structure: A Practical Approach* (Creighton, T. E., Ed.) pp 253−259, IRL Press, Oxford, U.K.
49. Buttry, D. A., and Ward, M. D. (1992) Measurement of interfacial processes at electrode surfaces with the electrochemical quartz crystal microbalance, *Chem. Rev. 92*, 1355−1379.
50. Buttry, D. A. (1991) Applications of the QCM to Electrochemistry, in *A Series of Advances in Electroanalytical Chemistry* (Bard, A., and Dekker, M., Eds.) pp 22−33, Marcel Dekker, New York.
51. Sauerbrey, G. (1959) Verwendung von Schwingquarzen zur Wägung dünner Schichter and zur Mikrowägung, *Z. Phys. 155*, 206−22.
52. Kanazawa, K. K., and Gordon, J. G. (1985) Frequency of a quartz microbalance in contact with liquid, *Anal. Chem. 57*, 1770−1771.
53. Martin, S. J., Granstaff, V. E., and Frye, G. C. (1991) Characterization of a quartz crystal microbalance with simultaneous mass and liquid loading, *Anal. Chem. 63*, 2272−2281.
54. Ron, H., Matlis, S., and Rubinstein, I. (1998) Self-assembled monolayers on oxidized metals. 2. Gold surface oxidative pretreatment, monolayer properties, and depression formation, *Langmuir 14*, 1116−1121.
55. Evans, S. D., Sharma, R., and Ulman, A. (1991) Contact angle stability: Reorganization of monolayer surfaces? *Langmuir 7*, 156−161.
56. Kinnear, K. T., and Monbouquette, H. G. (1997) An amperometric fructose biosensor based on fructose dehydrogenase immobilized in a membrane mimetic layer on gold, *Anal. Chem. 69*, 1771−1775.
57. Tian, L., Wei, W.-z., and Mao, Y.-a. (2004) Estimation of kinetics parameters for the adsorption of human serum albumin onto hydroxyapatite-modified silver electrodes by piezoelectric quartz crystal impedance analysis, *Anal. Sci. 20*, 623−627.
58. Weber, G. (1961) Excited States of Proteins, in *Light and Life Symposium* (McElroy, W., and Glass, B., Eds.) pp 82−107, John Hopkins University Press, Baltimore.
59. White, A. (1959) Effect of pH on fluorescence of tyrosine, tryptophan, and related compounds, *Biochem. J. 17*, 217−220.
60. Eftink, M. R., and Ghiron, C. A. (1976) Fluorescence quenching of indole and model micelle systems, *J. Phys. Chem. 80*, 486−493.
61. Eftink, M. R., and Ghiron, C. A. (1981) A comparison of fluorescence quenching and cluorescence decay studies with tryptophan, *Photochem. Photobiol. 33*, 749−752.
62. Smalley, J. F., Chalfant, K., Feldberg, S. W., Nahir, T. M., and Bowden, E. F. (1999) An indirect laser-induced temperature jump determination of the surface pKa of 11-mercaptoundecanoic acid monolayers self-assembled on gold, *J. Phys. Chem. B 103*, 1676−1685.
63. Voinova, M. V., Jonson, M., and Kasemo, B. (2002) 'Missing mass' effect in biosensor's QCM applications, *Biosens. Bioelectron. 17*, 835−841.
64. Plank, C., Zauner, W., and Wagner, E. (1998) Application of membrane-active peptides for drug and gene delivery across cellular membranes, *Adv. Drug Delivery Rev. 34*, 21−35.
65. Smith, A., and Helenius, A. (2004) How virus enter animal cells, *Science 304*, 237−242.
66. Nemerow, G. R. (2000) Cell receptors involved in adenovirus entry, *Virology 274*, 1−4.
67. Ohkuma, S., and Poole, B. (1978) Fluorescence probe measurement of the intralysosomal pH in living cells and the perturbation of pH by various agents, *Proc. Natl. Acad. Sci. U.S.A. 75*, 3327−3331.
68. Alberts, B., Bray, D., Lewis, J., Raff, M., Roberts, K., and Watson, J. D. (1994) *Molecular Biology of the Cell*, 3rd ed., Garland Publishing, New York.


BI0606243